Mobility of 180° domain walls in congruent $LiTaO_3$ measured using real-time electro-optic imaging microscopy

Venkatraman Gopalan[a)]
Department of Materials Science and Engineering and Materials Research Laboratory, Pennsylvania State University, University Park, Pennsylvania 16802

Stephan S. A. Gerstl
Center for Materials Science, Los Alamos National Laboratory, Los Alamos, New Mexico 87545

Amit Itagi
Department of Electrical and Computer Engineering, Carnegie Mellon University, Pittsburgh, Pennsylvania 15213

T. E. Mitchell and Q. X. Jia
Center for Materials Science, Los Alamos National Laboratory, Los Alamos, New Mexico 87545

T. E. Schlesinger and D. D. Stancil
Department of Electrical and Computer Engineering, Carnegie Mellon University, Pittsburgh, Pennsylvania 15213

(Received 12 February 1999; accepted for publication 19 April 1999)

We report the electric-field dependence of 180° domain-wall mobility in congruent $LiTaO_3$ measured at room temperature using *in situ* electro-optic imaging microscopy. The measured sideways domain-wall velocity of serrated domain fronts formed upon merger of domains was an order of magnitude larger than that for independently growing domains. The wall velocities also show a strong dependence on the nature of the applied electric field, being an order of magnitude larger for steady-state voltages as compared to pulsed voltage measurements. This is shown to be due to wall stabilization between applied voltage pulses resulting in an inertial delay in moving a domain wall which has been at rest for many seconds. © *1999 American Institute of Physics.* [S0021-8979(99)03215-6]

I. INTRODUCTION

Ferroelectric $LiNbO_3$ and $LiTaO_3$ are important materials for applications ranging from integrated and nonlinear optics,[1,2] to acoustic-wave devices,[3] pyroelectric detectors,[4] and holography.[5] All of these applications depend on the behavior of ferroelectric domains. Recent advances in understanding the 180° domain kinetics in ferroelectric $LiNbO_3$ and $LiTaO_3$ crystals have resulted from some important developments: first is the successful growth of stoichiometric $LiNbO_3$ and $LiTaO_3$ crystals with low coercive fields, indicating the critical role of lithium nonstoichiometry in influencing the domain kinetics in these materials.[6,7] This also corroborates other studies which collectively show a direct correlation between nonstoichiometry, large internal fields,[8,9] optical birefringence in the $x-y$ plane next to a domain wall,[10] and built-in strains and electric fields at a domain wall.[11] The second is the use of electro-optic imaging microscopy (EOIM) to study 180° domain-wall kinetics in real time under fields as large as 21 kV/mm.[12] This technique has enabled direct measurement of mobilities of 180° domain walls in these materials.

It was reported in Ref. 12 that the *in situ* measurement of domain mobility of independently growing domains in congruent $LiTaO_3$ is an order of magnitude larger than the values measured by pulsed voltage application followed by *ex situ* observation. It was further reported that, when independently growing domains merge, they form serrated fronts which move with a further order-of-magnitude increase in wall velocity. These studies were reported only at one constant electric-field value.

In this work, we have performed a systematic study of the sideways velocities of 180° domain walls in congruent $LiTaO_3$ as a function of applied electric field. We have performed wall velocity measurements under both steady-state voltages and pulsed voltages using EOIM. The previous measurements[13] of wall velocities using pulsed voltage measurements are indeed underestimated by an order of magnitude in the field regime studied here. The merged domain fronts also show a further order-of-magnitude increase in wall velocities at the fields studied here.

The article is organized as follows: In Sec. II we discuss the experimental observation of the 180° domain switching using EOIM. The domain-wall mobilities measured under steady-state voltage conditions are presented in Sec. III, and under pulsed voltage conditions in Sec. IV. The experimental results are discussed in Sec. V and conclusions are presented in Sec. VI.

II. EXPERIMENT

The following experiments were performed on congruent Z-cut $LiTaO_3$ crystals (obtained from Yamaju Crystals, Inc., Japan). The starting crystals were single crystal, single

a)Electronic mail: Vgopalan@psu.edu

domain, and in the form of 2 in. wafers which were 0.5 mm thick. We will refer to this crystal state as the virgin state.[8] Small pieces of size 10 mm×10 mm were cut from this single wafer. All the experiments described here were performed on samples cut from one wafer (to be denoted wafer F). The domains were inverted by applying an electric field at room temperature using liquid electrodes (saturated KNO_3 solution in water). The coercive field as determined by the transient current peak upon application of a ramping voltage was determined to be 207 kV/cm.

The technique of electro-optic imaging microscopy has already been discussed in detail in Ref. 12. We used a special holder to apply an electric field and at the same time observe the domain reversal in transmission mode using Nomarski interference contrast. The field which is applied to reverse the domains also gives rise to an index difference Δn_2 at the 180° domain wall through the r_{23} electro-optic coefficient. This index difference gives rise to scattering of light at the wall which is observed by EOIM. The area of the electrode was a circle of 4 mm diam. However, the area of observation using EOIM was only 0.97×0.73 mm at the center of this circular electrode. The video recording was performed with a camera and a regular VCR with 30 frames/s. The recorded film was digitized using a video card and software on a Power Macintosh, through which every frame could be extracted. The final resolution was ~6×6 μm pixel size, and the image size was 160×120 pixels.

Domain kinetics was studied under two applied electric-field conditions: (a) steady-state voltage application and (b) pulsed voltage application. In the steady-state voltage studies, a constant voltage was applied to the sample through the entire period of domain switching time. The results of this study are discussed in Sec. III. In the pulsed voltage studies, a series of voltage pulses were applied through the switching process, each pulse resulting in a partial reversal of domains under the electrode area. The results of these studies are discussed in Sec. IV. In both these studies, *in situ* video observation was used to study the domain kinetics using EOIM.

III. DOMAIN KINETICS UNDER A STEADY-STATE FIELD

The experiments performed in this study were on five different pieces of wafer F. All the studies reported here correspond to the first domain reversal of a crystal in the virgin state, called the forward poling.[13] The process of domain reversal was observed *in situ* at constant electric-field values applied as voltage steps. The samples are hereafter denoted as F207, F208, F210, F212, and F214, corresponding to electric fields of 206.9, 207.6, 210.0, 212.0, and 214.0 kV/cm, respectively. Simultaneous measurement of the transient current data along with the electro-optic imaging of the domain inversion process was performed.

A. Transient current and imaging data

As an example, Fig. 1 shows the applied step voltage and the transient current pulse resulting from the domain reversal process for sample F208. The switching time t_s is

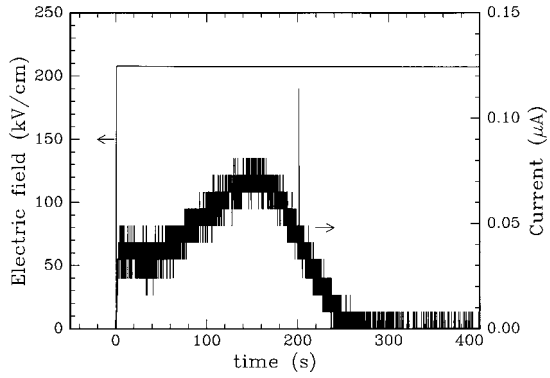

FIG. 1. Step voltage and the transient current during domain reversal in congruent *z*-cut $LiTaO_3$ while performing *in situ* domain imaging of sample F208. The arrows indicate the relevant axes for the plots.

~250 s. The switching times for domain reversal as obtained from the transient currents are plotted as a function of field for the five samples in Fig. 2. For comparison, we also show the switching times reported earlier for wafer B in Ref. 13. As discussed in that reference, there are two well-defined activation fields δ_f, for switching times, defined as[13]

$$t_f = t_{fo} \exp\left(\frac{\delta_f}{E_f - E_{\text{int}}}\right), \tag{1}$$

where E_f is the applied electric field in forward poling geometry.[13] An activation field of $\delta_f \sim 16\,500$ kV/cm for the low-field regime and $\delta_f \sim 30\,400$ kV/cm for the high-field regime was observed. These regimes also appear to be valid for wafer F as shown by the broken line fits. The internal field E_{int} in wafer F was measured[13] using transient current measurements to be 44.15 kV/cm.

B. Electro-optic imaging data

As an example, Fig. 3 shows a series of frames obtained from the electro-optic imaging data for the F208 sample. Only a selective collage of frames is shown in Fig. 3, although we could extract 30 frames per second from the video

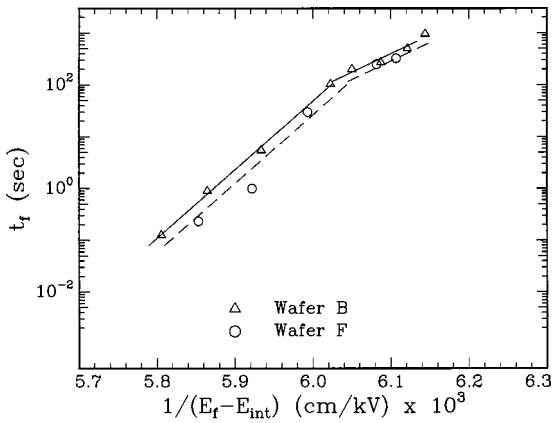

FIG. 2. Switching time t_f for forward poling of 180° domains in *z*-cut $LiTaO_3$ as a function of applied electric field E_f for this study on wafer F (circles) and from a previous study on wafer B (triangles). The internal field E_{int} is 44.15 kV/cm for wafer F and 42.20 kV/cm for wafer B.

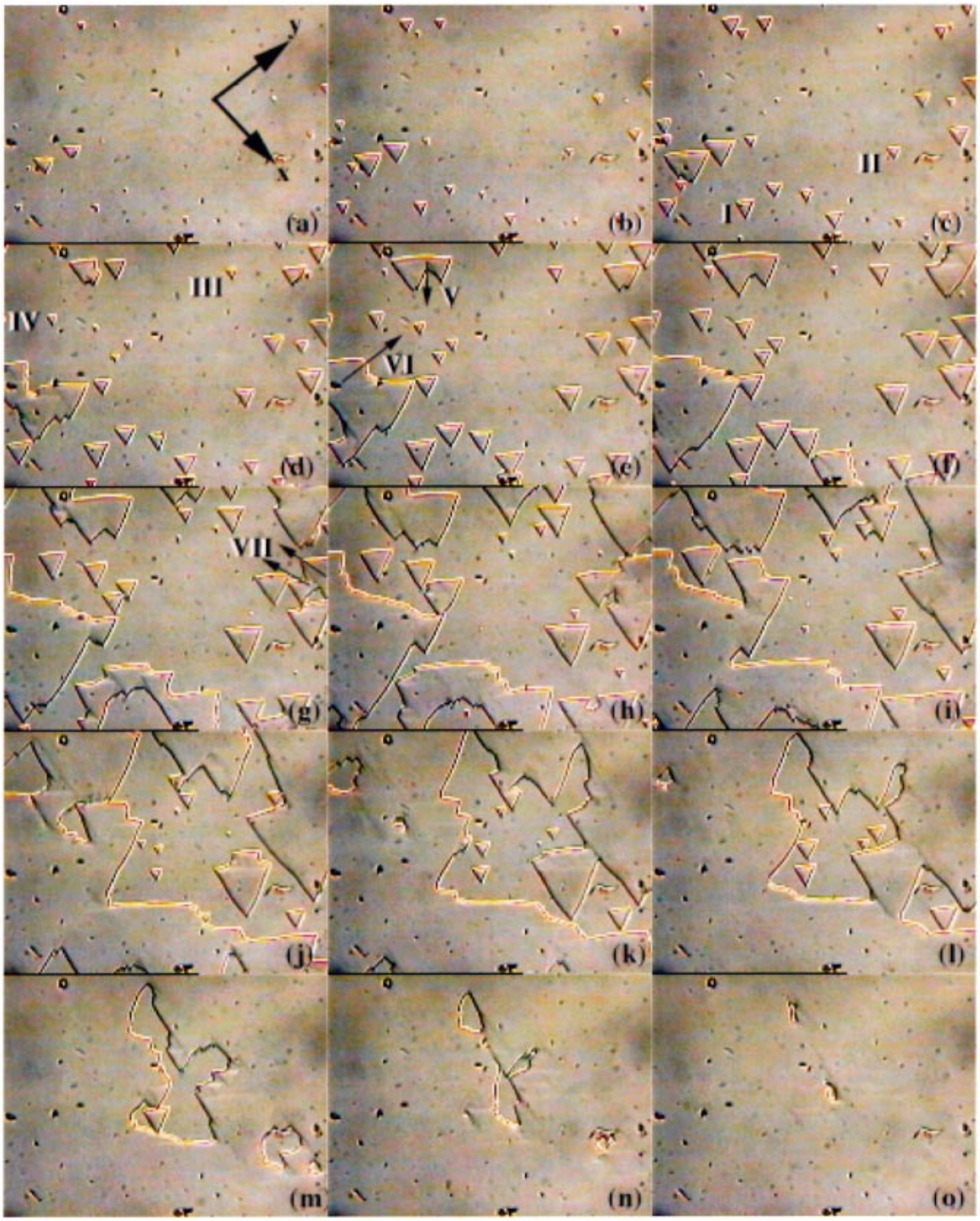

FIG. 3. Selected video frames from *in situ* recording of the nucleation and growth of 180° domains in congruent $LiTaO_3$ (sample F208) under an external field of 207.6 kV/cm (applied at time $t=0$ s) using EOIM. Frame (a) corresponds to $t=30$ s, and all successive frames [(b)–(o)] are 15 s apart from each other. The polarization axis is normal to the plane of the figure (the z plane) and the crystallographic x and y axes are marked. For independently growing domains (I, II, III, IV) and three merged domain fronts (V, VI, VII), for which domain mobilities were measured, are labeled. The arrows in frames (e) and (g) indicate the location and direction of the wall velocity measurement for the merged fronts V, VI, and VII.

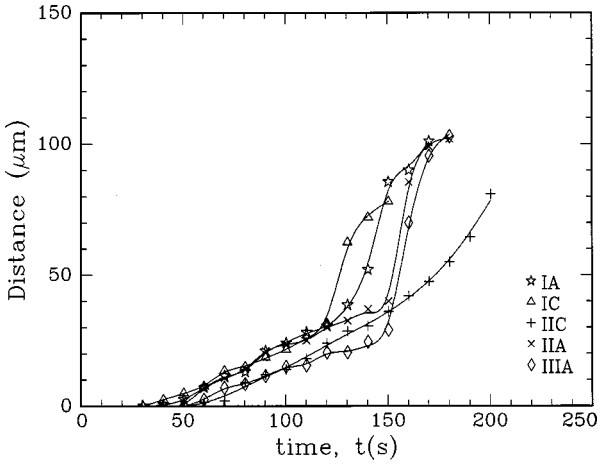

FIG. 4. Sideways movement of some representative 180° domain walls from Fig. 3 (sample F208) as a function of time after application of a steady-state electric field ($E_f = 207.6$ kV/cm) at $t = 0$ s. The notation IA, for example, stands for the measurements on side A of domain I in Fig. 3. The solid lines are drawn as guides to the eye.

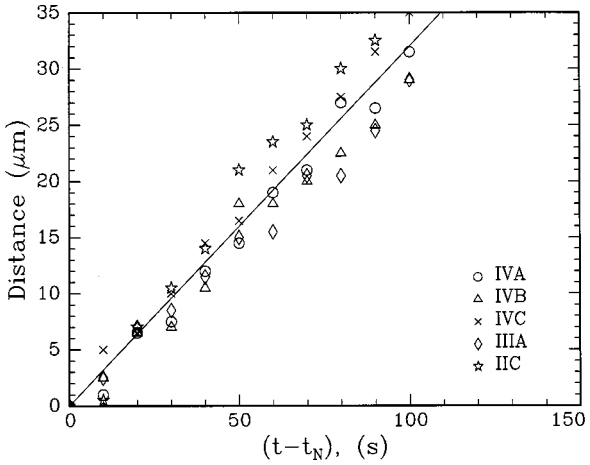

FIG. 5. Initial sideways movement of some representative 180° domain walls of independently growing domains III and IV in Fig. 3 (sample F208) as a function of time t under an external electric field $E_f = 207.6$ kV/cm applied at $t = 0$ s. The solid line is a straight line fit. The nucleation time t_N of domains II, III, and IV were 37.13, 48.23, and 59.83 s, respectively. The average sideways velocity is $v_{s,f} \sim 0.32\ \mu$m/s.

from the start of the voltage pulse to the end of the domain reversal process. If the step voltage was applied at time $t = 0$, the first frame (a) in Fig. 3 corresponds to $t = 30$ s. Every successive frame is spaced by 15 s and named 3(b), 3(c), 3(d), etc. The final frame is Fig. 3(o) and corresponds to $t = 240$ s. The polarization axis is normal to the plane of the image. The 180° domains nucleate and grow in the form of triangular domains with domain walls perpendicular to the mirror plane[5] [for example, domains I, II, III, and IV shown in Figs. 3(c) and 3(d)]. The crystallographic y axis corresponds to $[1\bar{1}00]$ and lies in the mirror plane. Eventually, the domains merge sideways and form a merged domain front like domains V, VI, and VII indicated in Figs. 3(e) and 3(g). The arrows indicate the location and direction of the sideways velocity measurement of these fronts, the results of which are presented in the next section.

Each frame in Fig. 3 is 160 pixels wide and 120 pixels high, with each pixel of size $6 \times 6\ \mu$m^2. The resolution with which we could estimate the position of the walls was within ~ 3 pixels. Assigning the bottom left-hand corner of every frame as pixel coordinate (0,0), we determined the origin of the triangular domains. For example, domain I originates at O_{I} (45,17) at a nucleation time $t_N = 21.83$ s and the origin of domain II is O_{II} (118,44) at $t_N = 37.13$ s. We label the three domain walls of each of triangular domains I as IA, IB, and IC as follows. Referring to the crystallographic x and y axes in Fig. 3(a), wall A is perpendicular to the y axis, and B and C follow anticlockwise around the triangle from wall A.

C. Sideways wall velocities

The average distance traveled by each of the walls from the origin O in a direction normal to the wall was measured. As a representative example, Fig. 4 shows the wall velocity for a number of walls in sample F208. In the initial stages after nucleation, the walls appear to move at a steady-state sideways velocity, as seen from the linear part of the distance–time curves in Fig. 4. However, around ~ 120 s after the start of the voltage step, the walls appear to show sharp rises in velocity, indicating a speeding up process. This is the first indicator of the presence of two regimes in sideways wall velocity of moving domains: First is the lower steady-state velocity ($v_{s,f}$) of independently growing triangular domains such as domains I, II, III, and IV, where subscript s stands for sideways velocity and subscript f for forward poling.[13] However, when these domains start merging with neighboring domains, they form serrated domain fronts such as V, VI, and VII, which move with a higher steady-state velocity ($v_{s,fm}$), where the subscript m stands for a merged front.[12] The sudden increases in the velocity of the individual domain walls in Fig. 4 correspond to discrete merging events. For example, referring to Fig. 3, domain I is growing independently until approximately frame 3(g) ($t = 120$ s), when it merges with two other domains. These two mergers around 120 s are reflected in the rise in velocities of edges IA and IC in Fig. 4.

The distance moved versus time after nucleation of some representative walls in the independently growing domains is plotted in Fig. 5 showing that, at a field of 207.6 kV/cm, the sideways velocity of independently growing domain walls is $\sim 0.32\ \mu$m/s. In order to measure the increased velocity of merging domains, we chose the merged domain fronts V, VI, and VII. Choosing an arbitrary point behind the moving front as the origin,[12] we measured the velocity of these fronts at various points along the front, as shown by arrows in Figs. 3(e) and 3(g). The results are plotted in Fig. 6, showing that they move at a higher steady-state velocity of $\sim 1.8\ \mu$m/s.

Similar measurements of sideways domain wall velocity ($v_{s,f}$) of independently growing domains and of merged domain fronts ($v_{s,fm}$) were also performed for samples F207, F210, and F212. The EOIM data obtained from sample F214 (corresponding to the highest field value in Fig. 2) were not useful due to lack of sufficient video frame rate. The EOIM data for sample F212 has been detailed in Ref. 12. These velocity measurements are plotted in Fig. 7 as a function of

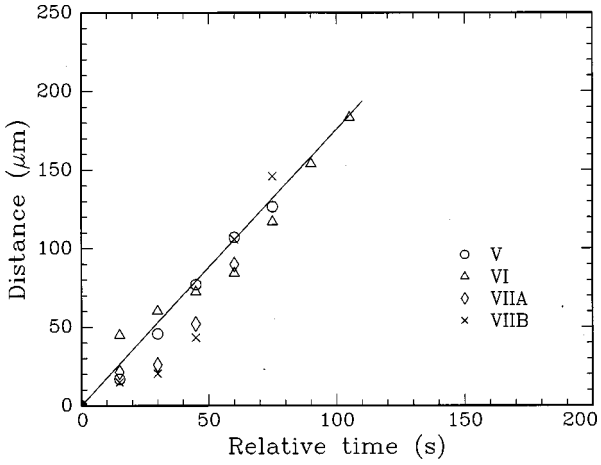

FIG. 6. Sideways movement of merged domain fronts V, VI, and VII in Fig. 3 (sample F208) under an external electric field of 207.6 kV/cm. The average velocity of the front is $v_{s,fm} \sim 1.8$ μm/s. The solid line is a straight line fit. The data VIIA and VIIB denote two measurements along the pair of arrows on domain front VII shown in frame (g) of Fig. 3.

applied electric field on a semilog plot to illustrate the relations[13]

$$v_{s,f} = v_{s,fo} \exp\left(- \frac{\alpha_{s,f}}{E_f - E_{\text{int}}} \right), \tag{2}$$

$$v_{s,fm} = v_{s,fmo} \exp\left(- \frac{\alpha_{s,fm}}{E_f - E_{\text{int}}} \right), \tag{3}$$

where $\alpha_{s,f}$ and $\alpha_{s,fm}$ are the activation fields for independently growing domain-wall velocity and merged front velocity, respectively. The measured values from Fig. 7 are $\ln(v_{s,fo}, \text{cm/s}) = 203.9 \pm 25.3$ and $\alpha_{s,f} = 35{,}200 \pm 4200$ kV/cm for independently growing domains, and $\ln(v_{s,fmo}, \text{cm/s}) = 237.8 \pm 20$ and $\alpha_{s,fm} = 40{,}500 \pm 3300$ kV/cm for merged domain fronts. These values of activation field are higher than the values for $\alpha_{s,f}$ reported earlier using pulsed voltage experiments followed by *ex situ* observation.[13] The actual magnitude of $v_{s,f}$ is significantly higher by an order of magnitude over previously reported results using pulsed voltage experiments. The merged front velocity is even higher. We will discuss these further in the discussion in Sec. IV.

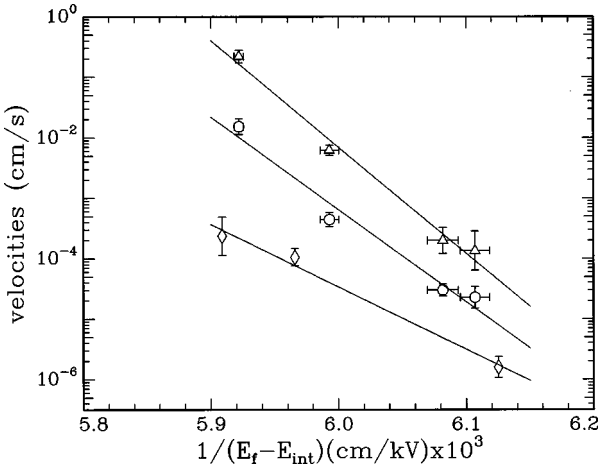

FIG. 7. Sideways wall velocities of 180° domain walls in congruent $LiTaO_3$ as a function of electric-field E_f measured using EOIM. The velocities $v_{s,f}$ of independently growing domains in wafer F are shown in circles and velocities $v_{s,fm}$ of merged domain fronts in wafer F as triangles. The sideways velocity $v_{s,f}$ from wafer B measured previously (Ref. 13) using pulsed voltage application followed by *ex situ* observation is also shown for comparison as rhombuses. The solid lines are straight line fits. The internal field E_{int} is 44.15 kV/cm for wafer F and 42.20 kV/cm for wafer B.

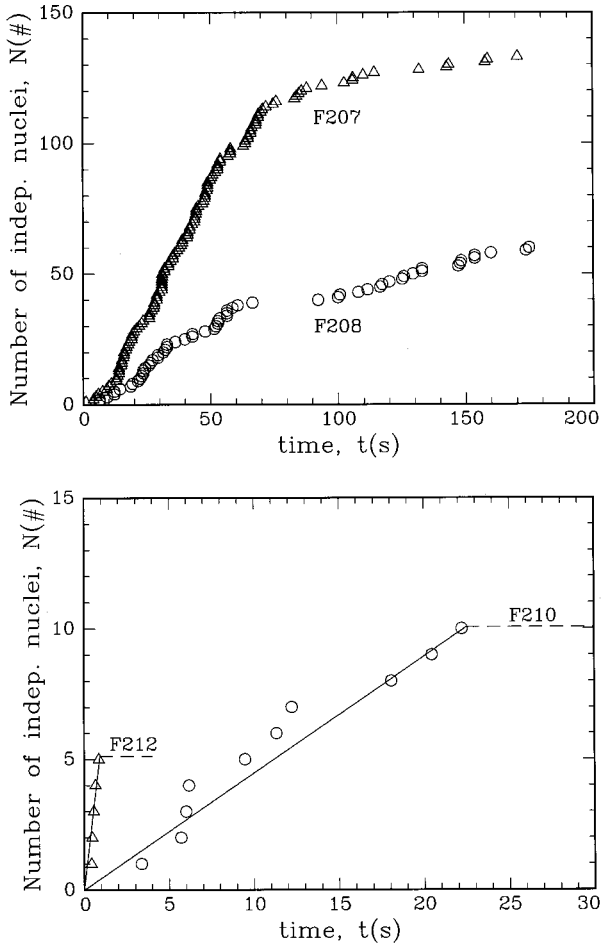

FIG. 8. Total number N of independently nucleating 180° domain nuclei as a function of time in the observation area (0.97×0.73 mm^2) of EOIM for (a) samples F207 ($E_f = 206.9$ kV/cm) and F208 ($E_f = 207.6$ kV/cm), and (b) samples F210 ($E_f = 210.0$ kV/cm) and F212 ($E_f = 212.0$ kV/cm). The fields were applied at time $t = 0$ s. Solid lines in (b) are straight line fits with the dotted line showing the saturation.

D. Nucleation rates

The numbers of independent nucleation events (N_f) in the video area were recorded as a function of time and are shown in Figs. 8(a) and 8(b). By independent nucleation events we mean those nuclei which nucleate in the original domain matrix independent of the presence of other domains around them. This would, for instance, preclude nucleation at a domain wall or on a merged front. The typical trend for this curve at all the fields studied here is an initial linear increase in the number of independent nuclei followed by a saturation where few new independent nucleations take place. This saturation value is denoted N_{sat}. The initial nucleation rate (N_f) and the saturation value of the number of nuclei (N_{sat}) for the video area is plotted as a function of field in Fig. 9. The saturation number of nuclei N_{sat} decreases with increas-

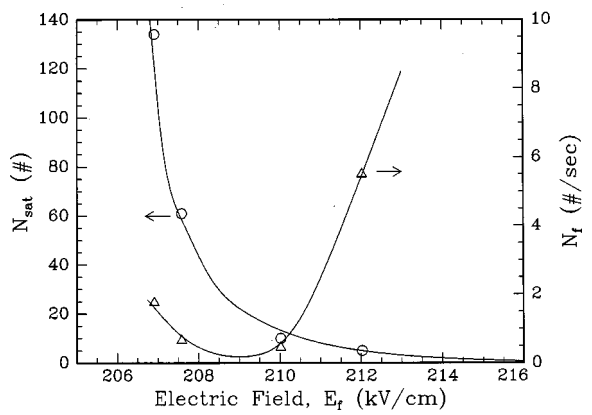

FIG. 9. Initial nucleation rate N_f (triangles) of independently nucleating 180° domains and the saturation number N_{sat} (circles) of domains as a function of electric field E_f measured from the data of Fig. 8. Solid lines are drawn as a guide to the eye. The arrows indicate the relevant axes for the plots.

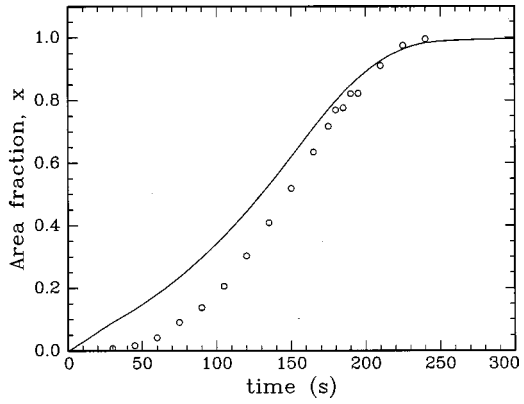

FIG. 10. Area-fraction x of growing 180° domains (sample F208) resulting from (a) integrating the current pulse of Fig. 1, shown as solid line, and (b) from the total area of the growing domains from EOIM images in Fig. 3, shown as circles.

ing field, as expected. However, the initial nucleation rate appears to show a small initial decrease before increasing with increasing field. These features will be discussed further in Sec. IV.

By the very nature of this measurement, we only include the nuclei which grow to be at least 1–2 pixels (6–12 μm) on the video screen. However, this measurement is of value since the domains which nucleate and grow for us to observe on the video screen are the ones which contribute significantly to the domain kinetics with regards to switching time and the area fraction of inverted domains. Although those nuclei which may be smaller than a pixel will not be counted here, if these nuclei do not grow to any reasonable size to be observed during the entire switching period, their contribution to the overall kinetics is negligible unless their combined area fraction is significant owing to their probable large numbers. We simply note here that we believe this is not the case. Our belief stems from the fact that using the nucleation rate and wall velocity data measured here, we can reasonably predict[14] the measured switching times (Fig. 2) using a computer code based on the Avrami model.[15] This suggests that the prominent role in switching is played by the nuclei which we observe to nucleate and grow.

E. Area fractions

The area fractions (x) of inverted domain regions as a function of time were measured from the video data of Fig. 3. This is shown for sample F208 in Fig. 10. Also shown for comparison is the area-fraction data derived from integrating the transient current in Fig. 1. It is seen that the area fraction obtained from the transient current shows the beginning of nucleation and growth well before it is reflected in the video data. This suggests that nucleation has a slight preference at the electrode edges where there is a higher density of field lines due to fringing fields.[12] This effect is observed in all the samples (for example, see Ref. 12 for data on sample F212). Since the video area is only $\sim 0.97 \times 0.73\,\mathrm{mm}^2$ at the center of the electrode region (4π mm^2), the edge effects are excluded in the video data.

The Avrami nucleation and growth model[15] gives the area-fraction x of growing triangles as a function of time t as

$$x = 1 - \exp(-K v_s^2 N_f t^N), \tag{4}$$

where K is a constant, v_s is the (assumed) constant steady-state velocity, and N_f is the rate of nucleation per unit area. A two-dimensional model for triangular growth gives $K = \sqrt{3}$ and the Avrami exponent $n = 3$. Replotting the data in Fig. 10 as $\ln[\ln(1/(1-x)]$ vs t, one obtains the slope of the curve as the Avrami exponent n. The video data for all the fields are plotted in this form in Fig. 11. For samples F207 and F208 with low fields, the Avrami exponent is 2.95 and 3.1, respectively, which is close to 3 as predicted by Eq. (4). However, at higher fields this exponent is continuously increasing with time and has a value of ~ 11 for the F212 sample ($E = 212$ kV/cm).

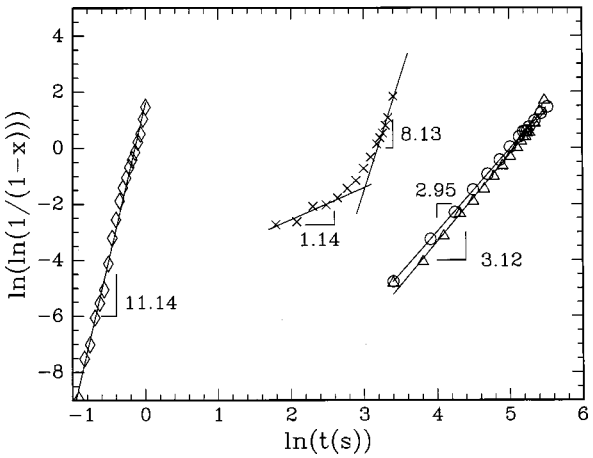

FIG. 11. Area-fraction x of the domain inverted region as a function of time for samples F207 (circles; $E_f = 206.9$ kV/cm), F208 (triangles; $E_f = 207.6$ kV/cm), F210 ($\times$'s; $E_f = 210.0$ kV/cm), and F212 (rhombuses; $E_f = 212.0$ kV/cm). The data are plotted such that the slope of the curves gives the Avrami exponent n from Eq. (4).

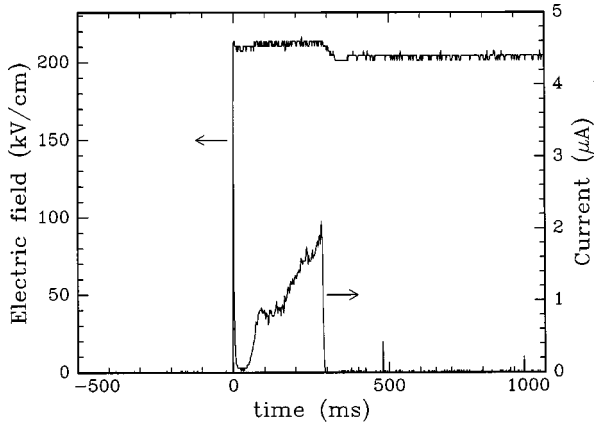

FIG. 12. Shape of the voltage pulse (300 ms wide; $E_f = 212$ kV/cm) with a base-line voltage of 205 kV/cm for measuring the wall mobility (sample F13) under pulsed voltage experiments. The transient current response upon domain reversal is also shown. The base-line voltage is below the coercive field (207 kV/cm) but helps domain-wall stabilization after the wall has moved under the influence of the 300 ms voltage pulse. The arrows indicate the relevant axes for the plots.

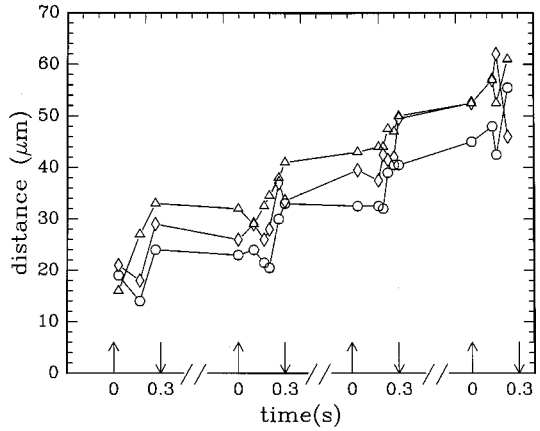

FIG. 13. Sideways movement of domain walls in independently growing 180° domains as a function of time upon application of voltage pulses as shown in Fig. 12. The movement of three sides of a triangular domain (shown by circle, triangle, and rhombus) in response to four successive pulses is shown. The start of a pulse is marked by an up arrow, and the end of the 300 ms pulse by a down arrow. The ''‖'' signs between the pulses indicates a time lapse of 30–40 s.

IV. DOMAIN KINETICS UNDER PULSED VOLTAGE APPLICATION

Figure 7 clearly shows that the independent domain-wall velocities measured by EOIM are an order of magnitude larger than those measured earlier by pulsed voltage measurements followed by *ex situ* optical observation.[13] In order to investigate the reason for such behavior, we performed pulsed voltage experiments on sample F13 from the same wafer F in combination with EOIM observation.

A. Pulsed voltages and transient currents

The pulsed voltage experiment was performed at an electric field value of 212 kV/cm, which corresponds to the same field as sample F212, and therefore, provides a comparison. Since the switching time at 212 kV/cm is ~1 s (Fig. 2), voltage pulses of 300 ms width were chosen for application. However, as reported earlier,[13] the stabilization time for 180° domains at room temperature is ~1.5–2 s, and therefore, a 300 ms pulse would result in a completely reversible domain-wall motion and result in no net change in domain microstructure. Therefore, a base-line field of 205 kV/cm was chosen for the pulse, as shown in Fig. 12. This base line was chosen quite arbitrarily as a field value below the coercive field at which no domain-wall motion was observed over many hours; the domain-wall motion is, therefore, arrested at the end of the 300 ms pulse. This is seen from the transient current response which goes to zero after the 300 ms pulse. However, the base-line field, which stays on for 10–20 s after the pulse, allows the domain stabilization process to occur.[13]

B. Sideways wall velocities

Figure 13 shows the movement of the three sides of an independently growing domain upon application of voltage pulses as shown in Fig. 12. Four of those voltage pulses (field of 212 kV/cm; 300 ms width each) are shown. The start of each pulse is shown by an up arrow and the end (300 ms) by a down arrow along the time axis. After the end of the 300 ms pulse, the base-line voltage was on for another 5–10 s, following which it was lowered to zero voltage. The time elapsed between independent pulses was 30–40 s, as indicated by ''‖'' signs between the pulses.

One can make some significant observations in Fig. 13:

(a) The resolution with which the movement of the domain wall is tracked is a pixel (~6 μm). Therefore, one cannot make conclusions about any significant backtracking of a domain wall after each pulse.

(b) A common trend is that the movement of a domain wall within a 300 ms pulse is negligible for most part of the pulse (50%–90% of the pulse width) followed by some significant movement near the very end of the pulse. By monitoring the voltage directly across the sample, the measured rise time was ~350 ns (much smaller than the pulse width), thus confirming that the initial delay in domain-wall movement is *not* due to the pulse rise time.

(c) In all, ~18 pulses were required to completely reverse the domain under the electrode area, which implies a switching time of ~5–6 s. This is 5–6 times the switching time measured with a steady-state voltage. The switching time here is defined as the time required to completely reverse the domain under the electrode area as observed by EOIM.

(d) The average velocity of a domain wall during each pulse as calculated by the *net* movement of the wall during the period of the pulse divided by the pulse width (300 ms) was measured to be ~34 μm/s. This value is also consistent with earlier measurement of ~10 μm/s for sideways velocity of domains in wafer B (Ref. 13) for the same switching time of 1 s under a steady field. This could also be inferred from Fig. 7 keeping in mind that a switching time of 1 s corresponds to a value of $\sim 5.88 \times 10^{-3}$ cm/kV for the inverse field $1/(E_f - E_{\text{int}})$ along the x axis.

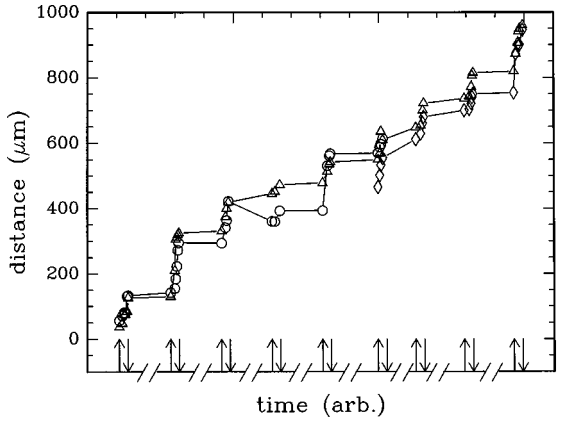

FIG. 14. Sideways movement of merged 180° domain fronts as a function of time upon application of voltage pulses as shown in Fig. 12. The movement of the domain front at three different points along the front is shown by triangles, circles, and rhombuses. Each applied pulse was 300 ms long. The start of a pulse is marked by an up arrow, and the end of the pulse by a down arrow. The ''‖'' signs between the pulses indicates a time lapse of 30–40 s.

Similar measurements were made for merged domain fronts with pulsed voltage application. Figure 14 shows the movement of a merged domain front made at three different locations along the front with application of voltage pulses. The average velocity of the merged front as measured by the *net* distance moved by the front during a pulse divided by the pulse width (300 ms) was measured to be $\sim 340\ \mu$m/s. We will discuss these observations in the next section.

V. DISCUSSION

In this section, we will discuss the following important observations: (1) The sideways velocities of independently growing domains measured by video are an order of magnitude faster than the velocities measured by pulsed voltage experiments. (2) When independently growing domains merge, they form serrated domain fronts which move with a further order-of-magnitude higher steady-state velocities. (3) The nucleation of independently growing domains at a constant field shows an initial linear increase with time N_f followed by saturation at a value N_{sat}. (4) The Avrami exponent for change in the area fraction of growing domains with time is close to 3 at lower fields but increases to very high values (>10) at higher fields.

A. Sideways wall velocity

The sideways velocity of 180° domains made under a steady-state electric field of 212 kV/cm (Fig. 5) was $\sim 200\ \mu$m/s for independently growing domains and $\sim 2300\ \mu$m/s for merged domain fronts. In contrast, the same measurement made using the pulsed voltage experiment at 212 kV/cm (Fig. 13) showed a velocity of $\sim 34\ \mu$m/s for independently growing domains and $\sim 340\ \mu$m/s for merged domain fronts. The switching time also increases from ~ 1 s under the steady-state electric field to $\sim 5-6$ s under pulsed voltage application at 212 kV/cm.

Therefore, two questions arise. First, why does the pulsed voltage measurement result in an underestimation of steady-state sideways velocity of both independent and merged domain fronts by an order of magnitude? Second, why is a merged domain front faster than independently growing domains by an order of magnitude?

Two possible explanations were presented in Ref. 12 towards answering the first question. One possibility was that there might be a considerable backtracking or ''inertial recoil'' of a moving 180° domain wall at the end of a voltage pulse. The data in Figs. 13 and 14 show that this inertial recoil, if any, has to be much less than a pixel movement ($\sim 6\ \mu$m) and is, therefore, not the predominant reason for the observed discrepancy in velocity measurements by steady-state and pulsed voltage measurements. The second possibility is that there exists an incubation period of as much as 90% of the pulse width during which time there is negligible movement of the domain wall. This explanation is borne out by the data in Fig. 13, which show that indeed most of the movement occurs only towards the end of the pulse. There is sufficient evidence now to conclude that the relaxation of point defect complexes arising from lithium nonstoichiometry in the vicinity of a polarization gradient at a domain wall is indeed responsible for internal fields,[8,9] optical birefringence,[10] electric fields, and strains of the order of 10^{-4} in the vicinity of a domain wall.[11] Therefore, the most plausible explanation for the incubation period required for the movement of a domain wall from rest is that when a domain wall comes to rest for a long time (much longer than the stabilization time of 1–2 s), it is stabilized by elastic and electrostatic relaxation of the lattice near the domain wall in response to the interaction of point defect complexes with the spontaneous polarization gradient. This would, therefore, suggest that the time scale of the measurement of domain kinetics in congruent $LiTaO_3$ in particular, and similar ferroelectrics in general, is crucial in interpreting the domain-wall mobility data reported in the literature.

The second question pertaining to the increased wall velocity of a merged domain front results from the formation of ledges upon domain merger. Based on simple energetics arguments, it was shown in Ref. 12 that the activation energy for nucleation at a ledge is lower than that for nucleation at a flat wall as on the sides of an independently growing domain. The formation of ledges upon merger, therefore, speeds up the domain front containing the ledges.

B. The nucleation rate

Figure 8 shows a time dependence for the nucleation rate at a constant field value. The general trend is that there is a linear increase in the total number of independently growing domains N with time t after the onset of a steady-state voltage followed by saturation at some constant value N_{sat}. Another general feature that is observed is that the onset of saturation in the total number of independent nuclei coincides with the onset of merging events between independently growing domains. This can be observed for sample F208 by comparing Figs. 4 and 8(a). This suggests that the saturation of the number of independent nuclei is related to the merging events. If we think of the initial nucleation rate N_{f} as the probability of nucleation per unit time, then the saturation of N implies that this probability tends to zero.

The probability of independent nucleation at any time t should be directly proportional to the untransformed area which is the area under the electrode where domain reversal has *not* yet taken place. Therefore, the probability N_f of nucleation per unit time should be directly proportional to the untransformed area. Since the untransformed area decreases with time and tends to zero after a time $t=t_s$, which is the switching time, the nucleation probability N_f also tends to zero. In other words, the probability of independent nucleations decreases with time because of the growth of the previously nucleated domains which overrun potential nucleation sites. These arguments should be true whether or not merging kinetics speed up the process of domain reversal. However, the merging accelerates this process by resulting in a faster decrease of the untransformed area with time and thereby giving a sharper saturation shoulder to the $N-t$ curves.

The magnitude of N_{sat} itself should decrease with higher electric fields as observed in Fig. 9, because of higher wall mobilities resulting in a faster overrunning of potential nucleation sites by fewer and fewer nuclei that nucleate at the start of the application of field. A higher electric field should result in a higher probability of nucleation per unit time. The initial nucleation rate N_{f}, however, shows a small initial decrease with field followed by a significant increase. Before we interpret this information, it must be noted that the data in Fig. 9 are based on four different video measurements at four field values. One of the assumptions in the measurement of nucleation statistics is that it is truly random spatially. In practice, this could be questioned for a small number of measurement statistics, and therefore, the initial drop in N_f in Fig. 9 needs to be reconfirmed with a statistically significant number of measurements before being subject to interpretation.

C. Avrami exponents

The Avrami model leads to Eq. (4) for the transformed area (or the domain reversed area) as a function of time at a constant electric field. The time exponent n, which is predicted to be 3 for the two-dimensional case in Eq. (4), is in reality a function of time and electric field and exceeds values of 10, as shown in Fig. 11. These apparent discrepancies relate to the fundamental assumptions made in the derivation of Eq. (4), which need to be reconsidered. The most important correction is that the sideways velocity $v_{s,f}$ at a given electric field is not a constant but rather a function of time. At the start of the domain reversal process, the sideways velocity of 180° domains is dominated by the growth of independent domains as shown by the data (as circles) in Fig. 7. After the merger of domains, the sideways velocity is dominated by merged domain fronts as shown by the data (as triangles) in Fig. 7. In the intermediate stages where both independent domains and merged domain fronts coexist, there is a distribution of velocities of domain growth.

At lower electric fields, the switching process is mainly dominated by the independently growing domains. In such a case, the time dependence of the sideways wall velocity can be ignored up until the very end of the switching period. Therefore, the assumption of a constant $v_{s,f}$ holds reasonably well in Eq. (4), and the time exponent n is close to 3 as predicted by the equation. This can be seen to be true for samples F207 and F208 in Fig. 11, which show an Avrami exponent of 2.95 and 3.11, respectively. At high fields, the merging kinetics become increasingly important, and the assumption of a constant $v_{s,f}$ with time breaks down.

The effect of domain growth due to electrode edges also affects the Avrami exponent, typically, lowering it due to a switch to a quasi-one-dimensional nucleation and growth problem along the edges.[16] However, in our EOIM measurements, we observe the kinetics only in a small area of $0.97 \times 0.73\,\text{mm}^2$ at the center of the electrode, which is a circle of 4 mm diam. The edge effects are, therefore, excluded from the measured data by EOIM. This is also reflected in the fact that the Avrami exponent obtained from the EOIM data for sample F208 is 3.11, while the same exponent obtained from the accompanying transient current data for the entire electrode area (see Fig. 10) is ~ 1.1 for the most part of the switching process ($\sim 70\%\ t_s$) and increases to ~ 2.9 toward the end of switching where merging dominates.

The issues of the time dependence of v_s and the influence of edge effects are presently being incorporated into the Avrami theory and tested using a numerical simulation code.

VI. CONCLUSIONS

The field dependence of 180° domain-wall mobilities in congruent $LiTaO_3$ were measured using *in situ* electro-optic imaging microscopy. The measured wall mobility of independently growing domains under a steady-state electric field were an order of magnitude higher than those measured by pulsed voltage application. This is shown to be related to wall stabilization between voltage pulses resulting in an inertial delay in the motion of the wall during the next pulse. The merged domain fronts show a further order-of-magnitude increase in wall mobility over the independently growing domains. This is related to the formation of ledges upon domain merger where further nucleation is preferred.

[1] L. E. Myers, R. C. Eckardt, M. M. Fejer, R. L. Byer, W. R. Bosenberg, and J. W. Pierce, J. Opt. Soc. Am. B **12**, 2102 (1995).
[2] K. Kinata, M. Fujimura, T, Suhara, and H. Nishihara, J. Lightwave Technol. **14**, 462 (1996).
[3] V. V. Lemanov and Yu. V. Llisavsky, Ferroelectrics **42**, 77 (1982).
[4] J. H. Lehman and J. A. Aust, Appl. Opt. **37**, 4210 (1998).
[5] S. Breer, K. Buse, K. Peithmann, H. Vogt, and E. Kratzig, Rev. Sci. Instrum. **69**, 1591 (1998).
[6] K. Kitamura, Y. Furukawa, N. Yasunori, V. Gopalan, and T. E. Mitchell, Appl. Phys. Lett. **73**, 3073 (1998).
[7] V. Gopalan, T. E. Mitchell, K. Kitamura, and N. Furukawa, Appl. Phys. Lett. **72**, 1981 (1998).
[8] V. Gopalan and M. C. Gupta, Appl. Phys. Lett. **68**, 888 (1996).
[9] V. Gopalan and M. C. Gupta, Ferroelectrics **198**, 49 (1997).
[10] V. Gopalan and M. C. Gupta, J. Appl. Phys. **80**, 6099 (1996).
[11] T. J. Yang, U. Mohideen, and M. C. Gupta, Appl. Phys. Lett. **71**, 1960 (1997).
[12] V. Gopalan and T. E. Mitchell, J. Appl. Phys. **85**, 2304 (1999).
[13] V. Gopalan and T. E. Mitchell, J. Appl. Phys. **83**, 941 (1998).
[14] A. Itagi, V. Gopalan, S. Gerstl, P. Swart, T. E. Schlesinger, D. D. Stancil, and T. E. Mitchell (unpublished).
[15] M. Avrami, J. Chem. Phys. **8**, 212 (1940).
[16] L. E. Levine, K. L. Narayan, and K. F. Kelton, J. Mater. Res. **12**, 124 (1997).